Surface and Interfacial Fourier Transform Infrared Spectroscopic Studies of Latexes. XVI. Quantitative Analysis of Surfactant in Multilayered Films

B.-J. NIU and MAREK W. URBAN*

Department of Polymers and Coatings, North Dakota State University, Fargo, North Dakota 58105

SYNOPSIS

Migration and concentration levels of sodium dioctylsulfosuccinate (SDOSS) surfactant molecules in 50%/50% styrene/butyl acrylate latex were detected at the film-substrate (F-S) and film-air (F-A) interfaces in mono- and double-layered films. For the purpose of quantitative analysis, absorption coefficients of the 1,056 and 1,046 cm^{-1} bands attributed to the $SO_3^-Na^+ \cdots HOOC$ and $SO_3^-Na^+ \cdots H_2O$ associations, respectively, were determined. Using group theory formalism, local geometries of the $SO_3^-Na^+$ hydrophilic groups of SDOSS can be predicted. The analysis is extended to the 1,261 and 1,209 cm^{-1} bands resulting from the S—O asymmetric stretching vibrations, due to the same $SO_3^-Na^+ \cdots HOOC$ and $SO_3^-Na^+ \cdots H_2O$ associations, and to the 1,290 and 1,236 cm^{-1} bands, due to asymmetric stretching modes of hydrophobic tails of the SDOSS. By the use of polarization attenuated total reflectance Fourier transform infrared (ATR FT-IR) experiments, these studies show that hydrophilic $SO_3^-Na^+$ ends on SDOSS are preferentially parallel to the film surface. At the same time, hydrophobic tails are perpendicular to the surface. The assessment of the amounts of SDOSS at the F-S and F-A interfaces was obtained by quantitative ATR FTIR analysis, which was extended to the silicone-modified double-layer latex films. In this case, the concentration of SDOSS molecules decreases as the depth of penetration increases. The highest concentrations of SDOSS molecules are detected at the shallowest depths near the surface of the top layer and the interfacial regions between the latex layers. © 1996 John Wiley & Sons, Inc.

INTRODUCTION

Attenuated total reflectance Fourier transform infrared (ATR FTIR) spectroscopy is one of the useful approaches for the surface and interfacial depth-profiling experiments of polymeric films.[1-4] The penetration depth, d_p, is often expressed by the following equation:[5]

$$d_p = \frac{\lambda}{2\pi(n_0^2 \sin^2\theta - n^2)^{1/2}} \quad (1)$$

where d_p is the penetration depth into the surface; n_0 and n are the refractive index values of the ATR crystal and the polymer, respectively; θ is the angle of incidence; and λ is the wavelength of electromagnetic radiation. Although at first glance, this relationship appears to be very useful, the depth of penetration depends on the wavelength of light and the angle of incidence. While the angle of incidence can be used to obtain information from various surface depths, the wavelength dependence may create problems. For example, eq. (1) is quite useful because, by changing the angle of incidence, θ, the depth penetration can be varied, and if one can compensate for the wavelength dependence, quantitative assessments could be made. However, eq. (1) exhibits important limitations because it was derived with an assumption that the examined specimen is homogeneous.[6] Therefore, any variation in the concentration or chemical makeup of a specimen will invalidate this relationship. Hence, it has

* To whom correspondence should be addressed.

Journal of Applied Polymer Science, Vol. 62, 1903–1911 (1996)
© 1996 John Wiley & Sons, Inc. CCC 0021-8995/96/111903-09

limited use in the depth-profiling experiments. In response to these concerns, we[7] developed algorithms that allow us to account for two important phenomena in ATR spectroscopy: for the optical effects at the sample-crystal interface and for sample inhomogenity. While the issues of the ATR spectra correction were disclosed in our earlier publications,[1,2] in an effort to apply eq. (1) to nonhomogeneous surfaces, the surface is numerically sliced to form a stack of parallel, thin homogeneous films.[2] By applying well-established reflectivity optical theory[8] to each layer and assuming that each layer is homogeneous, thus permitting the use of eq. (1), surfaces can be reconstructed by a stepwise treatment of the volumes occupied by each layer. As a result, one can obtain a distribution of the species for nonhomogeneous surfaces, particularly, a quantitative distribution of surfactants in the latex films.

In previous studies on latex films,[9-17] we have shown that there is a concentration gradient of sodium dioctylsulfosuccinate (SDOSS) surfactant near the film-air (F-A) and film-substrate (F-S) interfaces, but the actual quantitative aspect was left unanswered. In this study, we would like to revisit these issues and focus on a quantitative analysis of SDOSS molecules in silicone-modified polystyrene/poly(*n*-butyl acrylate) (Sty/*n*-BA) latex films. As was shown in the previous studies,[18] the SDOSS content is influenced by the presence of trimethoxysilyl propylmethacrylate (MSMA) siloxane. In an effort to quantitatively examine the distribution of SDOSS surfactant molecules in silicone-modified latex films, quantitative polarized ATR FTIR spectroscopy[1,2] will be used to analyze the content of the SDOSS molecules.

EXPERIMENTAL

In an effort to determine the extinction coefficients of the 1,046 and 1,056 cm^{-1} bands, the following experiments were conducted. Approximately 10 g of SDOSS surfactant was mixed with 1 mL of methacrylic acid (MAA) (Aldrich Chemical Co.). The mixture was cast on a thallium bromide-iodide (KRS-5) crystal, and the ATR FTIR spectra with TE (90°) and TM (0°) polarizations were recorded.[5] In another experiment, the SDOSS/MAA mixture was cast on a KRS-5 crystal, MAA was allowed to evaporate under air flow for 50 min, and the ATR FTIR spectra were recorded.

Polarized ATR FTIR spectroscopy was used to monitor the F-A and F-S interfaces of latex films. All ATR FTIR spectra were recorded on a Digilab FTS-20 instrument equipped with a rectangular ATR attachment (Spectra Tech) containing a KRS-5 crystal aligned to give an incident beam angle of 45°. In a typical experiment, 200 scans at a resolution of 4 cm^{-1} with TM and TE polarizer filter were collected. All spectra were transferred to an AT-compatible computer for further spectra analysis utilizing Spectra Calc software (Galactic Inc.). The spectra were corrected for optical effects by the use of a recently developed Q-ATR algorithm.[1,2]

For the determination of the extinction coefficients of SDOSS at 1,056 and 1,046 cm^{-1} bands, various concentration standards of SDOSS were prepared and ATR spectra were recorded with a Circle™ cell. The spectra were collected on a Mattson Cygnus 25 single-beam spectrometer (Sirrus 100) at a resolution of 4 cm^{-1} and with a mirror speed of 0.316 cm/sec. All circle ATR spectra were corrected by using the Q-ATR algorithm[1,2] to allow calculations of the extinction coefficients from the Beer-Lambert law.

RESULTS AND DISCUSSION

As previous studies[15-17] on *n*-BA/MAA indicated, the band at 1,050 cm^{-1} due to S—O symmetric stretching modes in $SO_3^-Na^+$ of SDOSS, splits to two bands at 1,056 and 1,046 cm^{-1}. The band at 1,056 cm^{-1} is due to the hydrogen-bonding associations of $SO_3^-Na^+$ groups with acid groups from latexes. On the other hand, the band at 1,046 cm^{-1} is due $SO_3^-Na^+$ groups associated with H_2O molecules. The ATR FT-IR spectra are shown in Figure 1, Traces B and C. For reference purposes, Trace A of Figure 1 illustrates the spectrum of SDOSS, and Traces B and C were recorded with TE and TM polarizations. Whereas the band at 1,056 cm^{-1} is attributed to the S—O stretching mode in the $SO_3^-Na^+$ end groups associated with acid groups from the latex copolymer, the band at 1,046 cm^{-1} is due to the S—O stretching modes resulting from water associations with $SO_3^-Na^+$. Although tentative assignments of the 1,056 and 1,046 cm^{-1} bands were proposed in our previous studies,[9-17] the origin of the 1,056 and 1,046 cm^{-1} vibrations will be addressed again because their intensities are sensitive to polarized light. For that reason, a formalism of the point group theory[16] will be considered. A primary motivation behind this effort is to be able to quantify the amount of SDOSS near the F-A and F-S interfaces.

With this in mind, let us consider Figure 2(A), which illustrates a hydrophilic $SO_3^-Na^+$ portion of

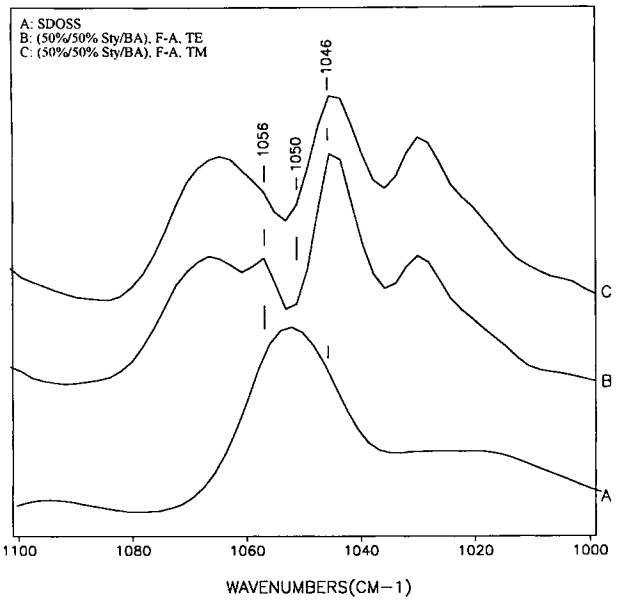

Figure 1 ATR FTIR spectra of the S—O symmetric stretching region. Traces: (A) pure SDOSS, (B) 100% *n*-BA with TE polarization, F-S interface, (C) 100% *n*-BA with TM polarization, F-S interface.

the surfactant end group. Neglecting the position of the Na^+ ion and assuming that all S—O bonds are equal, the point group of the free $SO_3^-Na^+$ is C_{3v}. On the basis of the group theory considerations,[19] vibrational modes for $SO_3^-Na^+$, with the C_{3v} point group, are $2A_1 + 2E$. A_1 is a symmetric mode, and E modes are doubly degenerated asymmetric modes. Following the character tables, one A_1 mode is IR active, which is detected at 1,050 cm^{-1}, and other IR-active E modes are detected at 1,216 cm^{-1} (see Trace A of Fig. 3). The other band due to double-degenerated E normal modes is detected at 581 cm^{-1} (not shown).

However, when the $SO_3^-Na^+$ environment is disturbed by the presence of the COOH acid and H_2O groups, the situation changes. Figure 2(B) shows the scenario when the surfactant molecules are associated with the acid groups via H-bonding. The point group for this structure is C_s, and following the selection rules, $4A' + 2A''$ are allowed vibrational modes in IR.

The structure of the SDOSS surfactant molecule associated with H_2O via H-bonding is presented in Figure 2(C). Similarly, the point group is C_s, and the allowed vibrational modes are $4A' + 2A''$, with six IR-active bands. Considering IR activity and the total number of bands for each local structure, it appears that these associations result in two asymmetric S—O stretching vibrations. The same situation occurs when water is present in the neighborhood of the $SO_3^-Na^+$ hydrophilic ends of the surfactant. Local symmetry is also C_s, thus allowing two asymmetric IR vibrations, but their vibrational energies will be different. Therefore, two bands at 1,261 and 1,209 cm^{-1} due to the S—O asymmetric stretching modes shown in Figure 3, Trace B, are detected, and the 1,056 and 1,046 cm^{-1} bands are the S—O symmetric stretching modes.

Although at this point, it would be appropriate to describe model experiments leading to the precise assignments of the SDOSS bands, let us first identify how each of the bands of interest behaves under TM and TE polarizations. The 1,056 and 1,046 cm^{-1} bands appear to be sensitive to the latex environ-

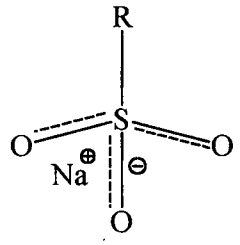

A: free $RSO_3^-Na^+$ (C_{3v})

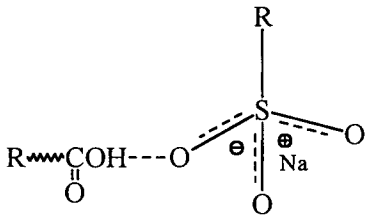

B: H-bonding association with acid group (C_s)

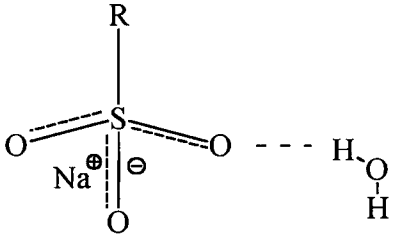

C: H-bonding association with H_2O (C_s)

Figure 2 Geometric diagrams of the $SO_3^-Na^+$ end. (A) Free $SO_3^-Na^+$ end, (B) H-bonding association with acid group, (C) H-bonding association with H_2O.

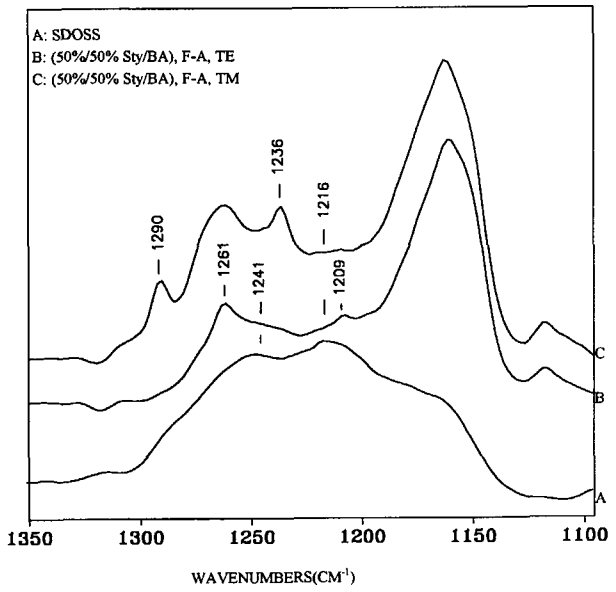

Figure 3 ATR FTIR spectra in the S—O asymmetric stretching region. Traces: (A) pure SDOSS, (B) 50%/50% Sty/BA, F-A, TE polarization, (C) 50%/50% Sty/BA, F-A, TM polarization.

ment, but in the case of the 50%/50% Sty/*n*-BA latex copolymer, with an approximate particle size of 100 nm, the situation changes. As illustrated in Figure 1, the band at 1,056 cm^{-1} is detected at the F-A interface when TE polarization is used (Trace B), but the same band is almost nondetectable in the TM polarization (Trace C). If the symmetric S—O stretching mode is affected by the polarization changes, let us examine a behavior of the S—O asymmetric stretching modes of the $SO_3^-Na^+$ end groups at the F-A interface in the 1,350–1,100 cm^{-1} region. This is illustrated in Figure 3, with Trace A showing an ATR FTIR spectrum of free SDOSS, with the bands at 1,241 cm^{-1}, due to the C—O asymmetric stretching mode, and at 1,216 cm^{-1}, due to the S—O asymmetric stretching modes. When SDOSS is placed in the latex environment, two bands at 1,261 and 1,209 cm^{-1} are detected at the F-A interface with TE polarization (Trace B). These bands are attributed to a splitting of the 1,216 cm^{-1} band from the S—O asymmetric stretching modes. They are, however, not detected in the TM polarization (Fig. 3, Trace C). Interestingly enough, the bands at 1,290 and 1,236 cm^{-1}, resulting from the splitting of the 1,241 cm^{-1} band due to C—O asymmetric stretching modes on SDOSS, are detected in TM polarization (Trace C).

These observations indicate that the $SO_3^-Na^+$ groups are preferentially parallel to the latex film surface when $COOH\cdots SO_3^-Na^+$ associations exist. The proposed structures are depicted in Figure 4(A). Since the band at 1,046 cm^{-1} is detected at both TE and TM polarizations and its intensity remains unchanged (Fig. 1, Traces B and C), the $SO_3^-Na^+$ groups associated with H_2O have no preferential orientation. This is because the acid groups of the latex copolymer are parallel to the latex surface, and therefore, the acid-associated SDOSS is also parallel.[12] This is shown in Figure 4(A). Since water molecules are small and not localized on the

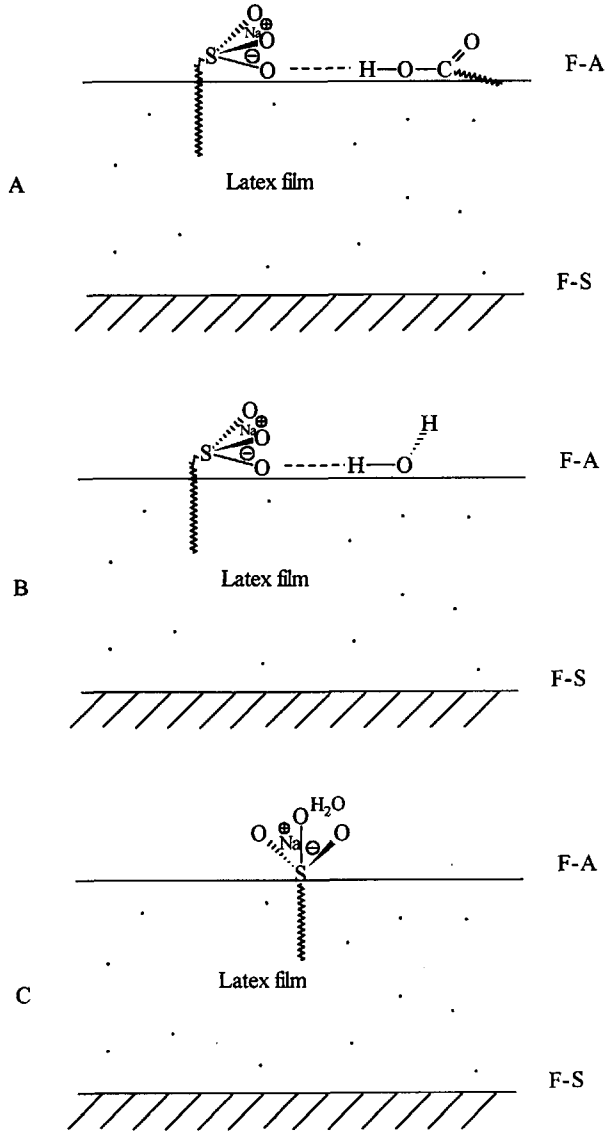

Figure 4 Proposed structures of SDOSS···MAA and SDOSS···H_2O associations. (A) $SO_3^-Na^+$ end group on SDOSS is parallel to the latex film surface, (B) $SO_3^-Na^+$ end group on SDOSS is parallel to the latex film surface, (C) $SO_3^-Na^+$ group is perpendicular to the latex film surface.

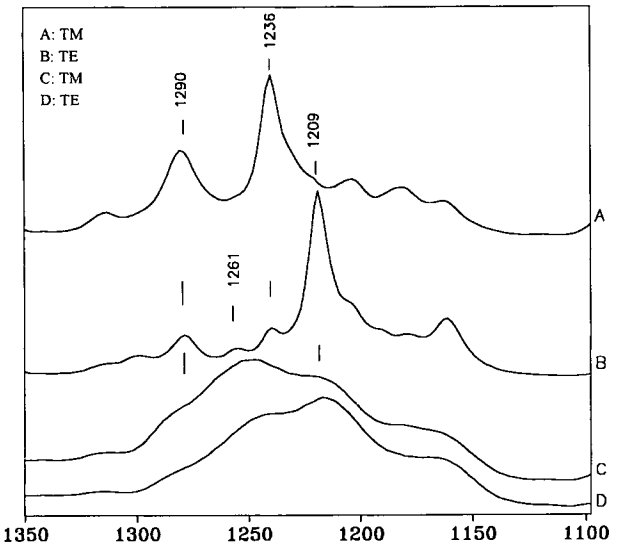

Figure 5 ATR FTIR spectra in the S—O asymmetric stretching region. Traces: (A) SDOSS/MAA mixture, TM polarization with 0 min drying time, (B) SDOSS/MAA mixture, TE polarization with 0 min drying time, (C) SDOSS/MAA mixture, TM polarization with 50 min drying time, (D) SDOSS/MAA mixture, TE polarization with 50 min drying time.

latex surface, there are two possible orientations for $H_2O\cdots SO_3^-Na^+$ associations, parallel and perpendicular. When the $SO_3^-Na^+$ groups associate with H_2O molecules which are deposited on the latex surface, the $H_2O\cdots SO_3^-Na^+$ entities appear to have parallel orientation. However, because of the hydrophobic nature of the surface, water molecules can be further away from the surface, thus forcing the $SO_3^-Na^+$ groups to be preferentially perpendicular. This is illustrated in Figure 4(B and C), respectively.

With this in mind, and in an effort to identify the origin of the SDOSS$\cdots$latex interactions, several model experiments were examined. For that reason, SDOSS was mixed with MAA. Traces A and B in Figure 5 are ATR FTIR spectra recorded immediately after the SDOSS/MAA mixture was deposited on a KRS-5 crystal. In a separate experiment, the SDOSS/MAA mixture was deposited on a KRS-5 crystal and MAA was allowed to evaporate. ATR FTIR spectra resulting from these experiments are illustrated in Figure 5, Traces C and D, respectively. Trace A of Figure 5 shows that the band intensities at 1,290 and 1,236 cm^{-1} are stronger when TM polarization is used. Both 1,290 and 1,236 cm^{-1} bands are due to the C—O asymmetric stretching modes of ester groups of an SDOSS molecule in two different environments, $SO_3^-Na^+\cdots HOOC$ and $SO_3^-Na^+\cdots H_2O$. Similarly, the 1,261 and 1,209 cm^{-1} bands are detected in the TE polarization (Fig. 5, Trace B) and are attributed to the S—O asymmetric stretching modes in the $SO_3^-Na^+$ in the two different environments.

The S—O symmetric stretching region is shown in Figure 6, with Traces A and B showing TM and TE polarizations, respectively. The presence of the 1,056 cm^{-1} band results from the S—O symmetric stretching modes of the $SO_3^-Na^+$ end groups due to SDOSS$\cdots$HOOC— associations. However, when MAA is removed from the SDOSS-MAA mixture, the band due to the S—O symmetric stretching mode is shifted to 1,046 cm^{-1}. This is shown in Figure 6, Traces C and D, and provides evidence that the nature of the SDOSS interactions changes when the acid groups are removed. When MAA is removed from the mixture, there are fewer $SO_3^-Na^+\cdots COOH$ associations, and hence, the bands at 1,290 and 1,261 cm^{-1} are not detected. For the same reasons, the bands at 1,236 and 1,209 cm^{-1} decrease (Fig. 5, Traces C and D).

Combining the results for asymmetric and symmetric S—O stretching modes, it is apparent that the decrease of the 1,290 and 1,261 cm^{-1} bands parallels a removal of MAA. At the same time, the band at 1,056 cm^{-1} is shifted to 1,046 cm^{-1}. Thus, the bands at 1,290 cm^{-1} is due to C—O asymmetric

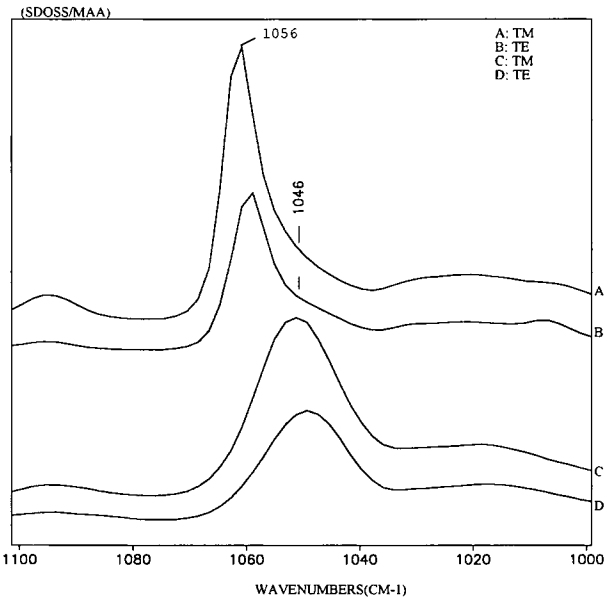

Figure 6 ATR FTIR spectra in the S—O symmetric stretching region. Traces: (A) SDOSS/MAA mixture, TM polarization with 0 min drying time; (B) SDOSS/MAA mixture, TE polarization with 0 min drying time, (C) SDOSS/MAA mixture, TM polarization with 50 min drying time, (D) SDOSS/MAA mixture, TE polarization with 50 min/drying time.

S—O stretching modes, the 1,261 cm^{-1} band is due to the asymmetric stretching modes, and the 1,056 cm^{-1} band results from the S—O symmetric stretching modes. All bands result from the SDOSS···HOOC— associations. On the other hand, the bands at 1,241 cm^{-1} (C—O asymmetric stretching), 1,216 cm^{-1} (S—O asymmetric stretching), and 1,046 cm^{-1} (S—O symmetric stretching) are attributed to the SDOSS···H_2O associations.

Having established the origin of the spectral features, let us attempt to quantify the amounts of SDOSS near the F-A and F-S interfaces. In an effort

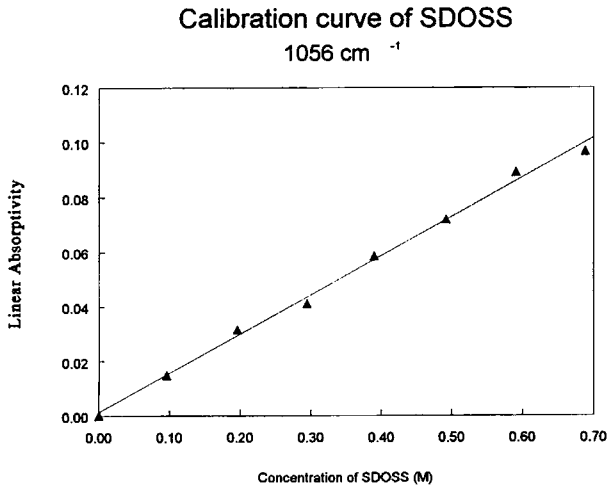

Figure 7A

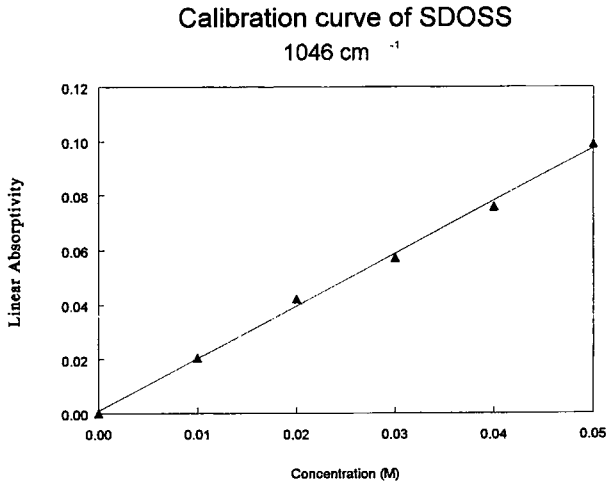

Figure 7 (A) A calibration curve of linear absorptivity at 1,056 cm^{-1} vs. concentration of SDOSS. (B) A calibration curve of linear absorptivity at 1,046 cm^{-1} vs. concentration of SDOSS.

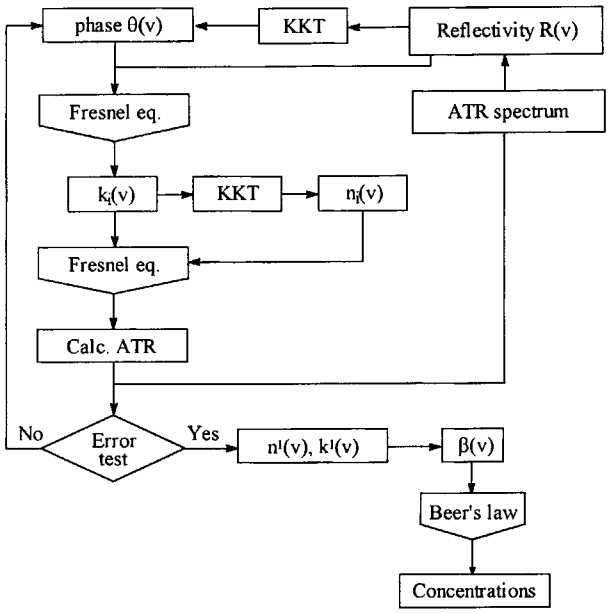

Figure 8 A schematic diagram of algorithm of depth penetration profiling analysis.

to do so at the F-A and F-S interfaces, it is necessary to obtain extinction coefficients for the bands of interest, in our case, the 1,056 and 1,046 cm^{-1} bands. For that reason, the plots of the 1,056 and 1,046 cm^{-1} band intensities as a function of concentration of SDOSS were constructed and are shown in Figure 7. In order to minimize the optical effects from the Circle™ ATR spectra, all spectra were corrected with the Q-ATR algorithm,[6] subsequently allowing calculations of the extinction coefficients from the Beer-Lambert equation:

$$\beta = \epsilon c \qquad (2)$$

where: ϵ (l/mol cm) is the extinction coefficient, c (mol/l) is the concentration, and β (cm^{-1}) is the linear absorptivity. From the Beer-Lambert equation, the extinction coefficient is the slope of the linear absorptivity versus concentration. The extinction coefficients were calculated from Figure 7(A) and (B) for the 1,056 and 1,046 cm^{-1} bands and are 0.14 and 1.9 l/mol cm, respectively. In an effort to quantify SDOSS at the interfaces, the absorbance index and reflective index spectra of SDOSS were incorporated in the depth penetration profiling analysis. A schematic diagram of the algorithm developed for the depth-profiling purposes is shown in Figure 8.[6]

According to eq. (1), the penetration depth depends on the wavelength of electromagnetic radiation and the angle of incidence. Because eq. (1) was

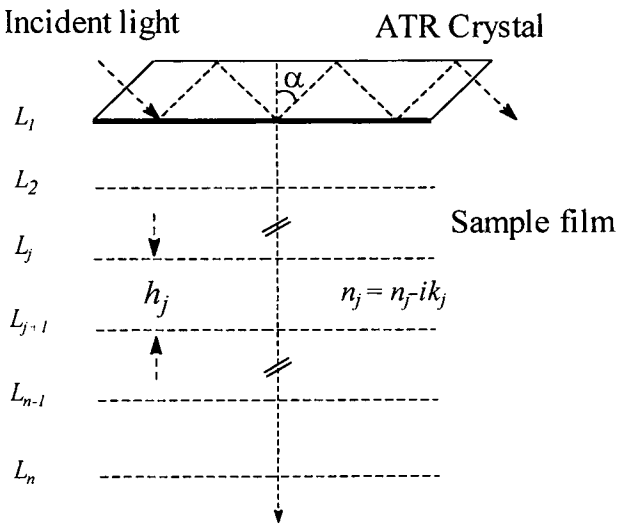

Figure 9 A schematic diagram of numerically slicing a nonhomogeneous surface to form a stack of parallel, thin homogeneous layers.

derived with an assumption that the examined specimens are homogeneous, any composition/concentration variations preclude the use of this useful relationship, especially if one is interested in the depth-profiling experiments. In order to apply this relationship for the quantitative analysis of nonhomogeneous surfaces, we developed an algorithm which allows us to overcome this problem.[6] Numerical details concerning its use were described elsewhere.[6] In essence, a nonhomogeneous surface is numerically sliced to form a stack of parallel, thin homogeneous films. This is schematically illustrated in Figure 9. The surface is divided into n layers, with each layer thickness, h_j. At the each boundary layer, L_j, the response of the sample to local evanescent waves can be characterized by a complex refractive index defined by $\hat{n}_j = n_j - ik_j$, where k_j is referred to as the absorption index.[2] By applying the Urban-Huang algorithm[2] to each layer, one can obtain information from each layer which is assumed to be homogeneous. This approach facilitates the use of eq. (1) to each layer, but the layers among themselves are not homogeneous. Using the approach of stacking all layers together, the surface is reconstructed by a stepwise treatment of the volumes occupied by each layer. This approach allows quite accurate quantitative analysis of surfaces, and its precision is determined by the number of spectra recorded at various depths.

Figures 10 and 11 illustrate a series of ATR FTIR spectra recorded as a function of the incidence angle, and it appears that the 1,056, 1,050, and 1,046 cm^{-1} bands change intensities as a function of the angle

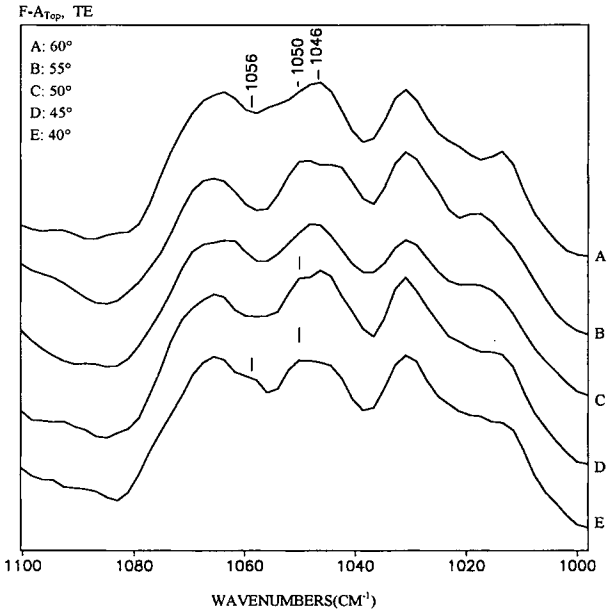

Figure 10 ATR spectra of the S—O symmetric stretching region recorded using a series of angles of incidence at the F-A_{Top} interface from two-layer latex film. Traces: (A) 60°, (B) 55°, (C) 50°, (D) 45°, (E) 40°.

of incidence. Using the calibration curves shown in Figure 7 and the algorithm shown in Figure 8, Figure 12 was constructed. Curves F-A and F-S are the concentration changes of SDOSS plotted as a func-

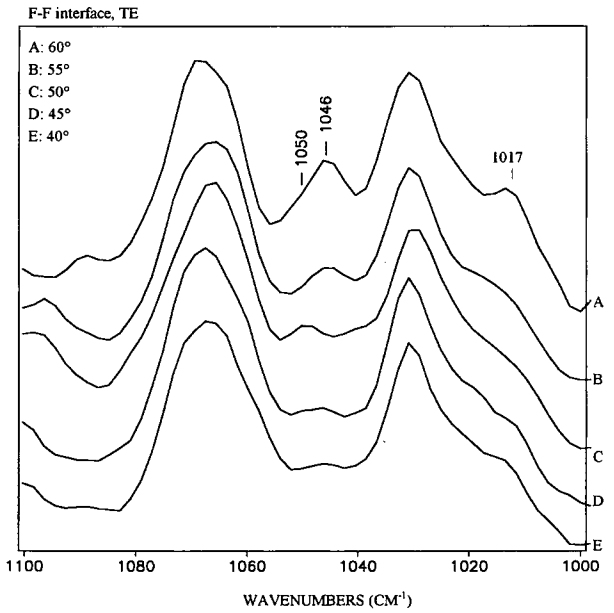

Figure 11 ATR spectra of the S—O symmetric stretching region recorded using a series of angles of incidence at the F-F interface from two-layer latex film. Traces: (A) 60°, (B) 55°, (C) 50°, (D) 45°, (E) 40°.

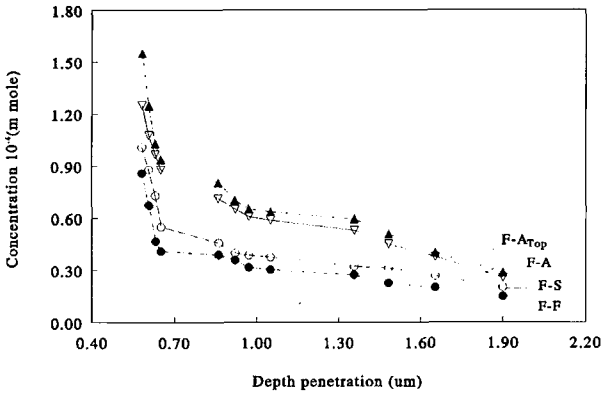

Figure 12 A plot of a quantitative amount of SDOSS molecules versus depth penetration at the F-A_{Top}, F-A, F-S, and F-F interfaces.

tion of the penetration depth near the F-A and F-S interfaces. These data illustrate that the SDOSS concentration diminishes very rapidly at shallow depths. However, it levels off when the penetration depth approaches 1.9 μm. The highest concentrations, 1.25×10^{-4} and 1.01×10^{-4} mmol, near the F-A and F-S interfaces, respectively, are detected at the depth penetrations near 0.58 μm. These values diminish to about 0.25×10^{-4} and 0.2×10^{-4} mmol at around 1.9 μm from the F-A and F-S interfaces, respectively. In order to minimize the interfacial surface tension, SDOSS molecules exude toward the interfacial regions, and the highest concentrations are detected close to the F-A and F-S interfaces, but the SDOSS concentration decreases at greater depths.

One of the issues that is of a particular interest is how the presence of multilayers will affect a distribution of SDOSS molecules across the film. For that reason, we designed an experiment in which one layer of latex was allowed to coalesce, followed by the deposition of another layer. The first layer was the one discussed above, and the layer deposited over the first one was modified with an MSMA silaxone. As a result, the F-A interface of the first layer becomes the film-film (F-F) interface, and the F-A interface of the overlayer will become the F-A_{Top} interface. The newly redefined F-A_{Top} and F-F interfaces in a double-layer latex film are schematically illustrated in Figure 13.

Because previous studies[9-18,20-22] indicated that there is a significant influence of silicone-containing polymers on the mobility of small molecules in latex films, we added 10% of MSMA to the latex aqueous suspension and examined how MSMA may influence the exudation of SDOSS molecules. By the use of the quantitative approach outlined above, the SDOSS concentration was monitored at the newly created F-F and F-A_{Top} interfaces and plotted as a function of the penetration depth from these interfaces. As indicated earlier, Curves F-A and F-S of Figure 12 show that the SDOSS concentrations near the F-A interface are higher than those at the F-S interface. This behavior can be attributed to the ability of SDOSS molecules to migrate preferentially toward the F-A interface. Our previous studies[17,18] also indicated that SDOSS migrations are influenced by the surface tension of a substrate and the glass transition temperature (T_g) of polymer/copolymer. For a higher styrene content, the T_g is higher and the rate of latex coalescence increases. The latter results from the increased water evaporation, likely due to the hydrophobic nature of styrene. Because SDOSS is water soluble, it will be carried out to the F-A interface. In this case, the effect of the surface tension of a substrate on "trapping" surfactant near the F-S interface is small. As a result, the higher SDOSS concentration is detected near the F-A interface. However, when another, modified with an MSMA, latex layer is added, the distribution of SDOSS within this new layer is affected by the addition of the MSMA molecules. As shown in Figure 12, the SDOSS concentration near the monolayer F-A interface is slightly lower than that detected near the F-A_{Top} interface after a layer of MSMA-modified latex was added (Curve F-A_{Top}). This observation indicates that more SDOSS molecules migrate toward the F-A_{Top} surface. On the other hand, a comparison of the SDOSS concentrations between the F-F and F-A_{Top} suggests that a higher content near the F-A_{Top} interface is detected (Curve F-A_{Top}); thus, fewer SDOSS molecules migrate toward the F-F interface because they are replaced by MSMA.

Let us recall Figure 11 (Trace A), with the band at 1,017 cm^{-1} due to the Si—O—C asymmetric stretching modes, detected at the F-F interface. Its presence indicates that the MSMA molecules are present near the F-F interface in a double-layer latex film. This observation is consistent with our previous studies,[18] which showed that the molecular-level

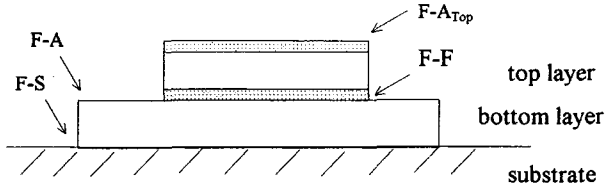

Figure 13 A schematic diagram of F-A_{Top} and F-F interfaces in the double-layer latex coalesced film.

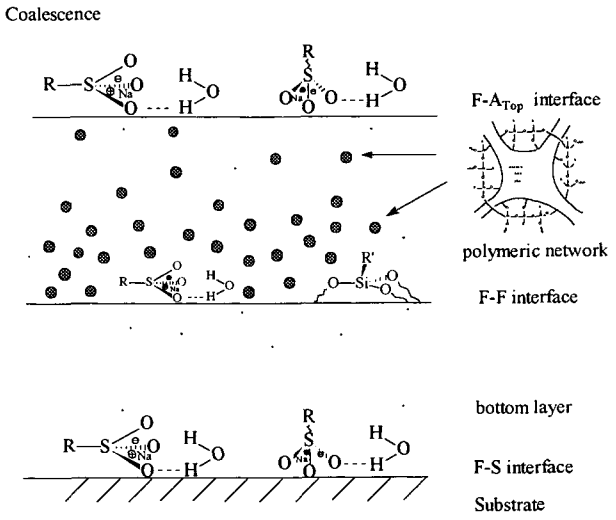

Figure 14 A schematic diagram of the possible molecular-level mechanism of MSMA during latex coalescence.

mechanisms responsible for the MSMA diffusion to interfaces are attributed to the formation of methoxy silanes near the substrate region. After hydrolysis, methoxy silanes are converted to hydroxyl groups, and during coalescence, covalent bonds between hydroxyl groups on MSMA and the latex are formed near the F-F interface. Thus, more MSMA are present near the F-F interface in the double-layer latex film, and higher concentrations of SDOSS molecules exude toward the F-A_{Top} interface in the double-layer latex films. The molecular-level mechanisms responsible for SDOSS and MSMA, along with the orientation changes, are schematically illustrated in Figure 14.

CONCLUSIONS

In this article, we presented a quantitative analysis of SDOSS distribution near the F-A and F-S interfaces in latex films. Analysis of IR spectra recorded from the MAA and SDOSS mixtures showed that it is possible to conduct model studies and determine the origin of the 1,056 and 1,046 cm^{-1} vibrations. They are due to the $SO_3^-Na^+ \cdots HOOC$ and $SO_3^-Na^+ \cdots H_2O$ associations, respectively. The extinction coefficients for these bands in this particular environment were also determined as 0.14 and 1.9 (l/mol cm), respectively. Combining analysis of the IR spectra as a function of penetration of depth allows one to quantify concentrations of SDOSS near the interfaces. The highest concentrations of the SDOSS molecules, 1.25×10^{-4} and 1.01×10^{-4} mmol, are detected near the F-A and F-S interfaces, respectively. In the case of silicone-modified double-layer latex films, the highest concentrations of SDOSS were 1.55×10^{-4} and 0.89×10^{-4} mmol, near 0.58 μm, for the F-A_{Top} and the F-F interfaces, respectively.

REFERENCES

1. J. B. Huang and M. W. Urban, *Appl. Spectrosc.*, **46,** 1666 (1992).
2. J. B. Huang and M. W. Urban, *Appl. Spectrosc.*, **47,** 973 (1993).
3. F. M. Mirabella, Jr., *J. Appl. Spectrosc. Rev.*, **21,** 45 (1985).
4. T. Hirayama and M. W. Urban, *Prog. Org. Coat.*, **21,** 81 (1992).
5. M. W. Urban, *Vibrational Spectroscopy of Molecules and Macromolecules on Surfaces,* Wiley-Interscience Publishers, New York, 1993.
6. M. W. Urban, *Attenuated Total Reflectance Spectroscopy of Polymers-Theory & Practice,* American Chemical Society, Washington, D.C., 1996.
7. N. J. Harricks, *J. Phys. Chem.*, **64,** 1110 (1960).
8. W. Hansen, *J. Opt. Soc. Am.*, **58,** 380 (1968).
9. M. W. Urban and K. W. Evanson, *Polym. Commun.*, **31,** 279 (1990).
10. K. W. Evanson and M. W. Urban, *J. Appl. Polym. Sci.*, **42,** 2287 (1991).
11. K. W. Evanson and M. W. Urban, *J. Appl. Polym. Sci.*, **42,** 2297 (1991).
12. T. A. Thorstenson and M. W. Urban, *J. Appl. Polym. Sci.*, **47,** 1381 (1993).
13. T. A. Thorstenson and M. W. Urban, *J. Appl. Polym. Sci.*, **47,** 1387 (1993).
14. T. A. Thorstenson, L. K. Tebelius, and M. W. Urban, *J. Appl. Polym. Sci.*, **49,** 103 (1993).
15. T. A. Thorstenson and M. W. Urban, *J. Appl. Polym. Sci.*, **50,** 1207 (1993).
16. J. P. W. Kunkel and M. W. Urban, *J. Appl. Polym. Sci.*, **50,** 1217 (1993).
17. B.-J. Niu and M. W. Urban, *J. Appl. Polym. Sci.*, **56,** 377 (1995).
18. B.-J. Niu and M. W. Urban, *J. Appl. Polym. Sci.*, to appear.
19. F. A. Cotton, *Chemical Applications of Group Theory,* 2nd ed.; Wiley-Interscience, New York, 1971.
20. J. Richard, C. Mignaud, and A. Sartre, *Polym. Int.*, **31,** 357 (1993).
21. E. P. Plueddemann, *Prog. Org. Coat.*, **11,** 297 (1983).
22. G. L. Witucki, *J. Coat. Tech.*, **65,** 57 (1993).

Received December 8, 1995
Accepted March 19, 1996